Available online at www.sciencedirect.com
ScienceDirect
Journal of Environmental Sciences 19(2007) 90–96
JOURNAL OF ENVIRONMENTAL SCIENCES
ISSN 1001-0742
CN 11-2629/X
www.jesc.ac.cn

Preparation, characterization and photocatalytic activities of boron- and cerium-codoped TiO_2

WEI Chao-hai[1,*], TANG Xin-hu[1,2,*], LIANG Jie-rong[2], TAN Shu-ying[2]

1. Institute of Environmental Science, South China University of Technology, Guangzhou 510640, China. E-mail: cechwei@scut.edu.cn
2. Department of Environmental Engineering, Jinan University, Guangzhou 510632, China. E-mail: ttangxh@sohu.com

Received 30 December, 2005; revised 7 March 2006; accepted 10 March, 2006

Abstract

Boron- and cerium-codoped TiO_2 photocatalysts were synthesized using modified sol-gel reaction process and characterized by X-ray diffraction (XRD), X-ray photoelectron spectroscopy (XPS), particle size distribution (PSD), diffuse reflectance spectra (DRS), and Brunauer-Emmett-Teller (BET). The photocatalytic activities were evaluated by monitoring the degradation of dye Acid Red B (ARB). The results showed that the prepared photocatalysts were mixed oxides mainly consisting of titania, ceria, and boron oxide. The structure of TiO_2 could be transformed from amorphous to anatase and then to rutile by increasing calcination temperature; the transformation being accompanied by the growth of particle size without any obvious change in phase structure of CeO_2. The XPS of $B_{1.6}Ce_{1.0}$-TiO_2 prepared at 500°C showed that a few boron atoms were incorporated into titania and ceria lattice, whereas others existed as B_2O_3. Cerium ions existed in two states, Ce^{3+} and Ce^{4+}, and the atomic ratio of Ce^{3+}/Ce^{4+} was 1.86. When boron and cerium were doped, the UV-Vis adsorption band wavelength showed an obvious shift toward the visible range ($\leqslant$526 nm). As the atomic ratio of Ce/Ti increased to 1.0, the absorbance edge wavelength increased to 481 nm. The absorbance edge wavelength decreased for higher cerium doping levels (Ce/Ti=2.0). The particles size ranged from 122 to 255 nm with a domain at 168 nm (39.4%). The degradation of ARB dye indicated that the photocatalytic activities of boron- and cerium-codoped TiO_2 were much higher than those of P25 (a standard TiO_2 powder). The activities increased as the boron doping increased, whereas decreased when the Ce/Ti atomic ratio was greater than 0.5. The optimum atomic ratio of B/Ti and Ce/Ti was 1.6 and 0.5, respectively.

Key words: titania; ceria; boron oxide; photocatalytic activity; Acid Red B

Introduction

Most investigations on heterogeneous photocatalysis focus on anatase-type TiO_2, because of its high photocatalytic activity under UV irradiation ($\lambda \geqslant 388$ nm), high chemical stability, and low cost (Hoffmann *et al.*, 1995; Licht *et al.*, 2000; Xie and Yuan, 2003). Considerable attention has been focused on inducing photocatalytic reaction under visible light (λ>400 nm) by doping transitional metal ions (Wang *et al.*, 2001; Yu *et al.*, 2003) or depositing some noble metals (Kamat, 2002; Li and Li, 2002; Bae and Choi, 2003), or coupling metallic oxides (Furube *et al.*, 1999; Reddy *et al.*, 2002b) into TiO_2 lattice. Recently, several investigators have doped nonmetal elements, e.g., N, S, and C, in the oxygen ion site of TiO_2 (Asahi *et al.*, 2001; Khan *et al.*, 2002; Ohno *et al.*, 2004). Some researchers have attempted to improve photocatalytic activities and realize visible light response by incorporating both metal ions and nonmetal elements into TiO_2 (Ishikawa *et al.*, 2002, 2004; Zhao *et al.*, 2004).

As an inexpensive and a relatively nontoxic material, ceria exhibits several characteristics that could be potentially advantageous for photocatalytic applications, and hence it has been applied to the photocatalytic elimination of organic pollutants, especially in combination with TiO_2 (Coronado *et al.*, 2002; Miyauchi *et al.*, 2002). It was reported that the UV-Vis absorbance edge wavelength of TiO_2 could be shifted toward visible range by doping Ceria, because of the substitution of Ti^{4+} for Ce^{3+}/Ce^{4+} at the interface between the two oxides (Liu *et al.*, 2005). The experimental results of Xie and Yuan (2004) showed that Ce^{4+}-TiO_2 colloid and nanocrystallites had the ability to degrade Reactive Red X-3B dye under visible light irradiation. On one hand, Otsuka-Yao-Matsuo *et al.* (2004) reported that the composite powder of $CeTiO_4$ with $SrTiO_3$ had relatively high photocatalytic activities under visible light irradiation (λ>420 nm). On the other hand, Jung *et al.* (2004) reported that the photocatalytic activity of B_2O_3-SiO_2/TiO_2 ternary mixed oxides was considerably influenced by the content of boron oxide. Incorporation of more than 10% of boron oxide caused a red shift of the light absorbance spectrum. Otherwise, a blue shift in the light absorbance band was observed because of the quantization of band structure. Zhao *et al.* (2004) clearly indicated that TiO_2 doped only with boron showed very low photocatalytic activity in the visible region.

Project supported by the National Natural Science Foundation of China (No. 20277010); *Corresponding author. E-mail: cechwei@scut.edu.cn.

The objectives of this study were to prepare boron- and cerium-codoped TiO_2, which were characterized using X-ray diffraction (XRD), UV-visible diffuse reflectance spectra (UV-Vis DRS), X-ray photoelectron spectroscopy (XPS), particle size distribution (PSD), and Brunauer-Emmett-Teller (BET), by a modified sol-gel method. The activities of the as-prepared photocatalysts were evaluated using the decomposition of Acid Red B (ARB), a representative azo dye.

1 Materials and methods

1.1 Synthesis of photocatalysts

The TiO_2 nanoparticle colloidal solutions were prepared using the controlled hydrolysis of tetrabutyl titanate and titanous trichloride (Zhao *et al.*, 2004). A calculated amount of boric acid and cerous nitrate were dissolved in 50 ml of anhydrous ethanol. After 1 h of vigorous magnetic stirring, 2.5 ml of tetrabutyl titanate and 2.5 ml of titanous trichloride were added with vigorous magnetic stirring under anaerobic conditions (purged with N_2). Sodium hydroxide solution (1 mol/L) was then slowly added to the solution, surrounded by ice bath. The clear solution was stirred at room temperature for 2 d. Subsequently, the gel that was formed was dried at 100°C. Finally, the pre-prepared samples were calcined at desired temperatures (300, 500, 700, or 900°C for 5 h. Pure, boron-doped and cerium-doped TiO_2 were prepared without adding boric acid and cerous nitrate under identical conditions, respectively. The prepared photocatalysts were named B_mCe_n-TiO_2, where m and n denoted the atomic ratio of B/Ti and Ce/Ti, respectively.

1.2 Characterization

The crystal phase of the prepared powder was studied by X-ray diffraction equipment with Cu K_α (Model XD-2, Microstructure Analytical Lab., Beijing, China) at room temperature. The accelerating voltage was 40 kV and the emission current was 20 mA. The UV-Vis DRS of the samples were obtained using a UV visible spectrophotometer (Model U-3010, Hitachi, Japan), and $BaSO_4$ served as a reference sample. To study the chemical state of dopants, the XPS spectra were collected with a PHI Quantum 2000 Scanning ESCA microprobe (Physical Electronics USA, a division of ULVAC-PHI, USA), using the Al K_α X-ray with the energy of 1486.6 eV and the working pressure of less than 5×10^{-7} Pa. The working potential and power of ion gun was 15 kV and 25 W, respectively. The PSD of the samples in water were examined using Zetasizer Nano S (Malvern Instruments Ltd., UK) at 25°C. The Brunauer-Emmett-Teller (BET), pore volume, and pore size were measured using ASAP2010 (Micromeritics Instrument Corporation, USA) with N_2 adsorption at 77.35 K. To investigate the surface properties of the prepared samples, the zeta potential values of photocatalyst suspensions at different pH values were measured using a zeta potential analyzer (Model JS94G+, Powereach Ltd., Shanghai, China).

1.3 Evaluation of photocatalytic activities

The photocatalytic activities of the prepared powder were investigated by monitoring the decomposition of ARB (Shanghai Dyestuff Chemical Plant, Shanghai, China), which was used without further purification. Fig.1 shows the molecular structure of ARB. Fifty milliliters of aqueous solution containing ARB dye (25 mg/L), the pH of which was adjusted to the desired value by adding hydrochloric acid or sodium hydroxide, was added to a 100-ml beaker placed on the top of a magnetic stirrer. A total of 0.05 g of photocatalyst was then added into the beaker. Irradiation was performed using a 30-W Philips UV lamp. The primary radiation wavelength of this lamp was 253.7 nm, and the incident light intensity at the level of solution was 0.2 mW/cm^2. During the reaction, 3 ml of suspension sample was collected at a specific time and filtered using Millipore 0.22 μm film. The concentration of ARB dye in the filtrate was determined by a Hitachi U-3010 Spectrophotometer.

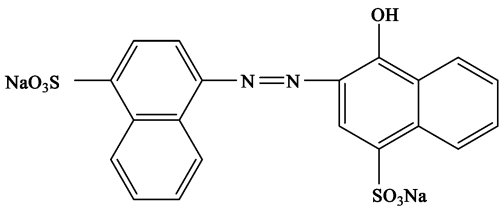

Fig. 1 Molecular structure of Acid Red B.

2 Results and discussion

2.1 XRD patterns

The XRD patterns for $B_{1.6}Ce_{1.0}$-TiO_2 calcined at different temperatures, as shown in Fig.2, indicated that the crystal phase composition of the photocatalysts depended on the calcination temperature. When calcined at 300°C, the amount of crystallites was too little, and hence no remarkable diffraction peaks were produced in the XRD profiles (Fig.2a). As the calcination temperature increased to 500°C, the diffraction (101) peak of anatase TiO_2 (ICDD PDF: 84-1286) and (111), (200), (220), (311) peaks of cubic CeO_2 (ICDD PDF: 81-792) appeared, as shown in Fig.2b. However, because the sample was not well crystallized, other diffraction peaks were too weak to be indexed.

The XRD patterns for samples calcined at 700 and 900°C showed that the TiO_2 phase in the photocatalyst transformed from the anatase to the rutile structure (ICDD PDF: 65-192), according to the (110), (101), (111), (211), and (301) peaks in Fig.2c and Fig.2d, and the other main peaks (331), (422), (511), and (531) of cubic CeO_2 could also be identified. Moreover, the diffraction peaks of TiO_2 and CeO_2 became sharper and more intense with the increase in calcination temperature, which indicated the progress of the formation and growth of the crystallites.

On the basis of the XRD profiles, the mean crystallite

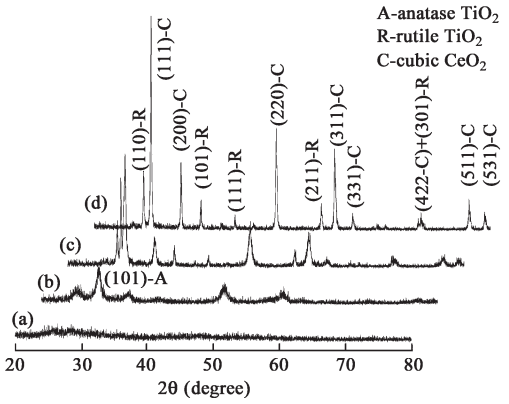

Fig. 2 XRD patterns of $B_{1.6}Ce_{1.0}$-TiO_2 calcined at 300°C (a), 500°C (b), 700°C (c) and 900°C (d).

sizes of samples calcined at different temperatures were calculated using the Scherrer equation, according to the full-width at half-maximum (FWHM) (in radians) of (101) peak for anatase, (110) peak for rutile, and (111) peak for cubic CeO_2. The results are summarized in Table 1.

2.2 XPS analysis

Fig.3 shows the XPS spectra of the O1s, B1s, Ti2p and Ce3d of $B_{1.6}Ce_{1.0}$-TiO_2 sample calcined at 500°C. As shown in Fig.3a, at least two kinds of oxygen species were present in the photocatalyst, because the O1s spectrum was asymmetric and could be well fitted into two peaks using XPSPEAK4.1 software package by eliminating the effect of the background count using the Shirley's method. Considering the difference in the electronegativity of the elements involved and the results in literature (Bensalem *et al.*, 1995; Reddy *et al.*, 2002a), the dominant peak at 529.83 eV could be assigned to metallic oxides, which was in agreement with binding energy of O1s electron arising from ceria and titania lattice. Another O1s peak at 531.91 eV was attributed to the surface hydroxyl group (Bensalem *et al.*, 1995; Liu *et al.*, 2005). Fig.3b shows that the XPS spectra of B1s was asymmetric and could be fitted into two peaks. The dominant peak at 192.04 eV (labeled A) was characteristic of B–O bonds in B_2O_3 (Harris *et al.*, 2002), and the weaker peak observed at 190.64 eV (labeled B) corresponded to B–Ti and B–Ce bonds (Harris *et al.*, 2002; Lu, 2004). It indicated that a few boron atoms were incorporated into TiO_2 and CeO_2 lattice, and others existed as B_2O_3. Fig.3c shows the Ti2p XPS spectra. The spin-orbit components ($2p_{3/2}$ and $2p_{1/2}$) of Ti2p spectra were deconvoluted by two curves (458.55 and 464.32 eV), corresponding to Ti^{4+} in a tetragonal structure (Lu *et al.*, 2000). It indicated that the Ti element existed as Ti^{4+} on the basis of the principle and instrument handbook of XPS (Galtayries *et al.*, 1998).

The Ce3d XPS spectra were known to be complex because of hybridization of the Ce4f with ligand orbitals and because the valence 4f orbitals were partially occupied (Park and Ledford, 1996; Reddy *et al.*, 2002a) (shown in Fig.3d). It could be assigned to $3d_{3/2}$ spin-orbit states (labeled u) containing five main peaks at 899.05 (u0), 900.08 (u), 903.80 (u1), 907.93 (u2), 916.55 (u3), and $3d_{5/2}$ states (labeled v) containing five main peaks at 881.02 (v0), 882.18 (v), 884.94 (v1), 889.85 (v2), 898.08 eV (v3). According to the experimental results (Park and Ledford, 1996; Liu *et al.*, 2005), the peaks labeled v, v2, and v3 were attributed to the primary photoemission from Ce^{4+}–O_2; hybridization between the O2p level and the Ce4f screening level resulted in v and v2 which were a mixture of $(5d\ 6s)^0 4f^2 O2p^4$ and $(5d\ 6s)^0 4f^1 O2p^5$ configurations, whereas v3 was a pure $(5d\ 6s)^0 4f^0 O2p^6$ final state. Structures v0 and v1 were attributed to a mixture of $(5d\ 6s)^0 4f^2 O2p^4$ and $(5d\ 6s)^0 4f^1 O2p^5$ configurations in Ce_2O_3. The structures labeled u, because of the Ce $3d_{3/2}$ levels, could be explained in the same manner (Li *et al.*, 2005b). The Ce3d spectrum of $B_{1.6}Ce_{1.0}$-TiO_2 sample basically denoted a mixture of Ce^{3+}/Ce^{4+} oxidation states and showed a myriad of peaks, indicating that Ce^{3+} was partially oxidized. The atomic ratio of Ce^{3+}/Ce^{4+} was about 1.86, according to the calculation using the corresponding peak areas. Nevertheless, diffraction peaks for Ce_2O_3 were not found in Fig.2, thereby indicating that Ce_2O_3 might be amorphous.

2.3 Optical absorbance

The UV-Vis DRS of $B_{1.6}Ce_{1.0}$-TiO_2 calcined at 300, 500, 700, and 900°C are shown in Fig.4, which showed that the UV-Vis adsorption band wavelength shifted to the visible range when boron and cerium were doped, and the intensity of absorbance decreased with the increase of the calcination temperature. Furthermore, the absorbance above 400 nm showed a significant increase for the samples calcined at 300 and 500°C, compared with the DRS of photocatalysts prepared at 700 and 900°C, although the anatase was transformed to the rutile structure and the band gap energy decreased.

Because the electronic structure of anatase TiO_2 was an indirect transition, the square root of absorbance coefficient was linear with photon energy. The band gaps of these samples were calculated from their diffuse reflectance by plotting the transformed Kubelka-Munk equation: $(F(R_\infty)\cdot E)^{1/2}$ versus the energy of light ($E=h\nu$) (Yakuphanoglu and Arslan, 2004), as shown in Fig.5.

Table 1 Crystal composition, mean crystallite sizes, and d-spacing of $B_{1.6}Ce_{1.0}$-TiO_2

Calcination temperature (°C)	Crystal composition		Crystal size (nm)		d-Spacing (nm)	
	TiO_2	CeO_2	TiO_2	CeO_2	TiO_2	CeO_2
300	Amorphous	Amorphous	—	—	—	—
500	Anatase	Cubic	6.7	13.9	0.3506 (101)	0.3106 (111)
700	Rutile	Cubic	69.9	29.8	0.3247 (110)	0.3116 (111)
900	Rutile	Cubic	83.5	59.8	0.3246 (110)	0.3123 (111)

"—" Denoted that the result could not be calculated.

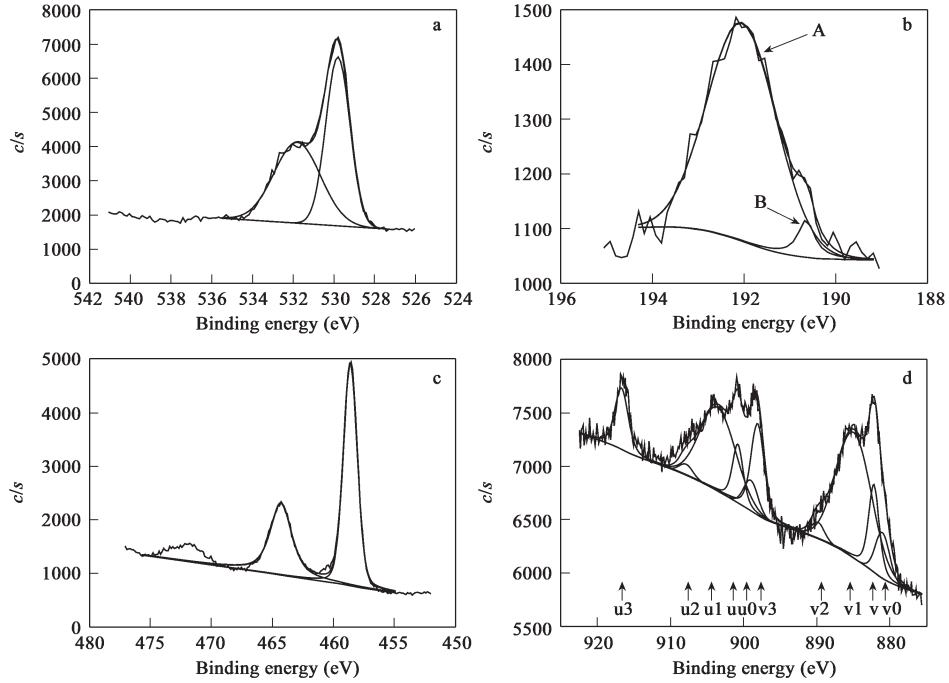

Fig. 3 O1s (a), B1s (b), Ti2p (c) and Ce3d (d) XPS spectra of $B_{1.6}Ce_{1.0}$-TiO_2 calcined at 500°C.

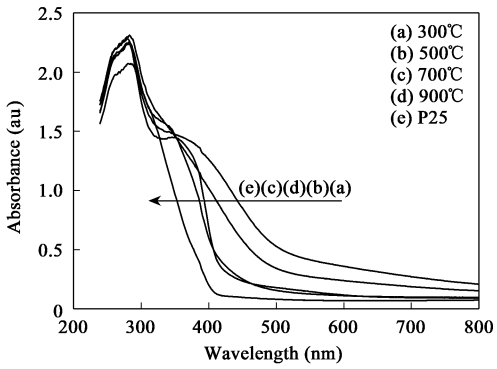

Fig. 4 UV-Vis DRS of $B_{1.6}Ce_{1.0}$-TiO_2 and P25.

Extrapolating the linear region of the transformed spectra to zero, the optical band gap energies of 2.36 eV (526 nm), 2.58 eV (481 nm), 2.93 eV (424 nm), 2.98 eV (417 nm) were obtained for $B_{1.6}Ce_{1.0}$-TiO_2 calcined at 300, 500, 700, and 900°C, respectively. These band gap energies were lower than those of P25 (3.2 eV). In terms of the stability of photocatalyst, the calcination temperature of 500°C was recommended.

To investigate the effects of cerium doping on the absorbance edge wavelength, the DRS of the samples doped with different cerium dosages are given in Fig.6. Compared with P25, the absorbance edge wavelength shifted to the visible region. With the atomic ratio of Ce/Ti increasing to 1.0, the absorbance edge wavelength increased. However, for higher doping levels (Ce/Ti = 2.0), the absorbance edge wavelength slightly decreased. As mentioned previously, Ti^{4+} ions could occupy the $Ce^{3+/4+}$ sites to form an interfacial phase. It could be considered an impurity band of interfacial with *n*-type identity. Red shifts of photocatalysts could be attributed to the charge transfer between the impurity band and the conduction band of TiO_2 (Xu *et al.*, 2002; Liu *et al.*, 2005). As discussed above, by plotting $(F(R_\infty)\cdot E)^{1/2}$ versus the energy of light, the optical band gap energies of 3.14 eV (395 nm), 3.00 eV (414 nm), 2.86 eV (434 nm), 2.58 eV (481 nm), and 2.68 eV (463 nm) were obtained for $B_{1.6}Ce_{0.0}$-TiO_2, $B_{1.6}Ce_{0.1}$-TiO_2, $B_{1.6}Ce_{0.5}$-TiO_2, $B_{1.6}Ce_{1.0}$-TiO_2 and $B_{1.6}Ce_{2.0}$-TiO_2, respectively.

2.4 PSD and BET analysis

The particle sizes of photocatalyst might vary over quite a wide range. The PSD for $B_{1.6}Ce_{1.0}$-TiO_2 sample calcined at 500°C was determined and given in Fig.7. It had a single-modal distribution characteristic, and the particle size distributed from 122 to 255 nm with a domain at 168 nm (39.4%). The percentage of 150–190 nm was ca. 85%. However, the PSD of photocatalyst sample was considerable different from the result calculated by Scherer equation, because the photocatalyst particles in the

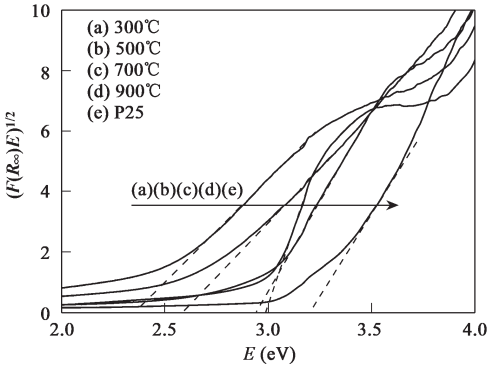

Fig. 5 $(F(R_\infty)\cdot E)^{1/2}$ versus photon energy for $B_{1.6}Ce_{1.0}$-TiO_2 and P25.

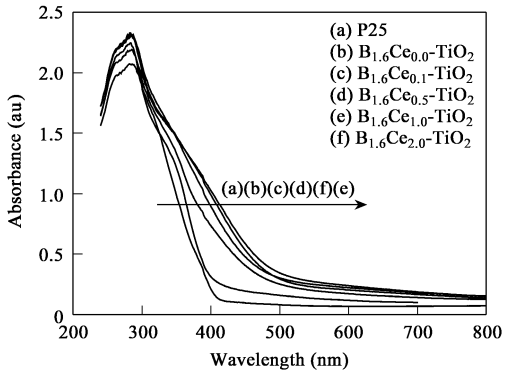

Fig. 6 UV-Vis DRS for the photocatalysts doped with different dosages of cerium.

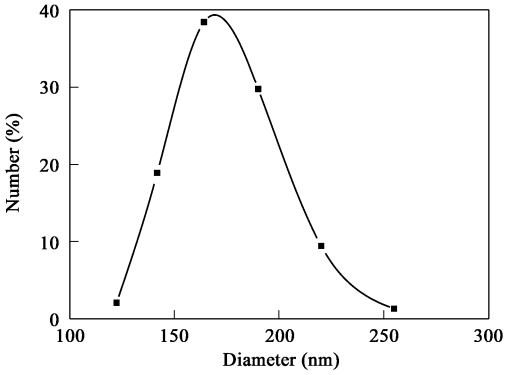

Fig. 7 PSD of the $B_{1.6}Ce_{1.0}$-TiO_2 sample suspension.

aqueous medium had obvious tendency to aggregate and generate larger particles.

The specific surface area, adsorption cumulative surface area of pores, adsorption cumulative pore volume, and adsorption average pore diameter for $B_{1.6}Ce_{1.0}$-TiO_2 sample were measured by BET method, and the results were 45.76 m^2/g, 46.02 m^2/g, 0.13 cm^3/g, and 11.05 nm, respectively. To investigate the effects of doping of cerium and boron ions on the pore structure and adsorption abilities of the photocatalyst, the nitrogen gas adsorption/desorption isotherm and the pore-size distribution tests were carried out, and the experimental results are shown in Fig.8. The adsorption isotherms (Fig.8a) demonstrated a pattern of Type IV curves (Li *et al.*, 2005a), which was a typical feature of porous materials. Fig.8b shows that the pore sizes of catalysts were distributed in the range of 1.94–93.27 nm and the catalysts had a dominant pore size of 7.57–31.97 nm. The percentage of pore volume with the sizes of 1.94–7.57, 7.57–31.97, and 31.97–93.27 nm was 15.2%, 71.0%, and 13.8%, respectively.

2.5 Effects of pH on the degradation of ARB dye

Fig.9 indicated that the photocatalytic degradation of ARB over $B_{1.6}Ce_{1.0}$-TiO_2 was remarkably affected by the solution pH. The degradation rate of ARB decreased drastically with an increase of pH. 94.3% and 83.5% of the removal rate of ARB were accomplished at pH 1.5 and pH 3.0, respectively, after 10 min of UV irradiation. However, only 19.6% and 1.1% of ARB were degraded at pH 5.0 and 7.0, respectively. Many researchers had reported that the photocatalytic reaction rate followed the Langmuir-Hinshelwood kinetics model, and adsorption was a "key step" for the photocatalytic degradation of organic pollutants. The adsorption of ARB over TiO_2 depended on the surface charge of TiO_2 particles. To investigate the surface properties of TiO_2 particles in water, the zeta potential values of photocatalyst suspensions as a function of pH were determined. The results showed that the pH of zero point of charge (pHzpc) of $B_{1.6}Ce_{1.0}$-TiO_2 sample was 4.88. When pH was higher than 4.88, the surface potential of $B_{1.6}Ce_{1.0}$-TiO_2 particles was negative. Whereas in an acqueous medium, an ARB molecule was ionized into an ARB anion and two sodium cations. The electrostatic repulsion between ARB anion and photocatalyst particles increased and the adsorbed amount of ARB decreased with increase of pH, resulting in decrease in ARB degradation. It was noteworthy that the positions of both valence and conduction band depended on the pH of the solution, and the potential of the valence and conduction bands shifted to 59 mV more toward the negative potentials as the pH increased by one unit at 25°C (Ward *et al.*, 1983).

2.6 Effects of boron and cerium dosages on photocatalytic activity

The photocatalytic activities of TiO_2 doped with different dosages of boron and cerium were measured by monitoring the degradation of ARB shown in Fig.10.

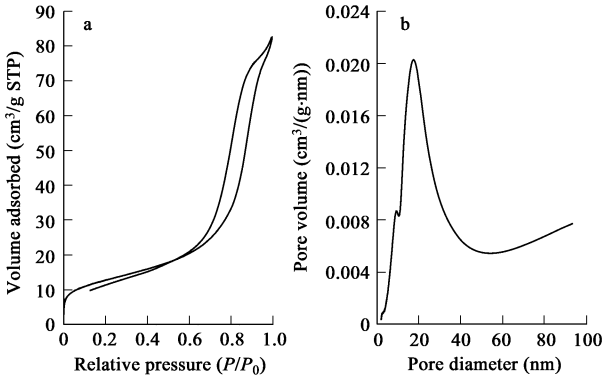

Fig. 8 Adsorption/desorption isotherm(a) and pore size distribution(b) of $B_{1.6}Ce_{1.0}$-TiO_2 calcined at 500°C.

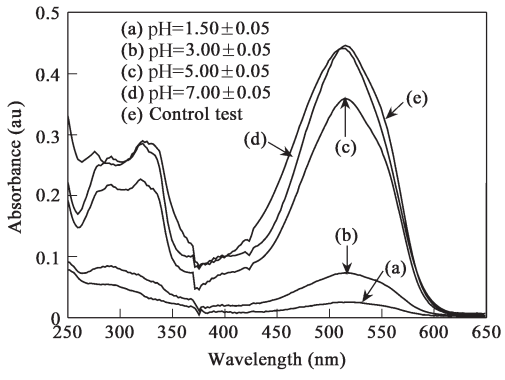

Fig. 9 Effects of pH on the degradation of ARB. Irradiation time=10 min; [ARB] =25 mg/L; [photocatalyst] = 1.0 g/L.

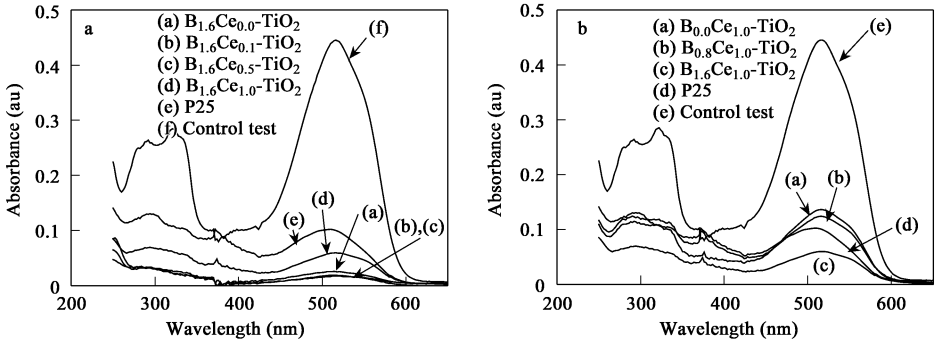

Fig. 10 Effects of cerium (a) and boron (b) dosage on the photocatalytic activities. Irradiation time=10 min; [ARB]=25 mg/L; [photocatalyst]=1.0 g/L; pH=3.0.

Fig.10a shows that the elimination of ARB were ca. 94.2%, 95.7%, 96.0%, 86.6%, and 77.1% over $B_{1.6}Ce_{0.0}$-TiO_2, $B_{1.6}Ce_{0.1}$-TiO_2, $B_{1.6}Ce_{0.5}$-TiO_2, $B_{1.6}Ce_{1.0}$-TiO_2 and P25, respectively, after 10 min of UV irradiation. It indicated that the photocatalytic activities of photocatalysts increased slightly with the increase in cerium dopant, when the atomic ratio of Ce/Ti was ⩽0.5. However, for greater atomic ratio of Ce/Ti, the photocatalytic activities showed an obvious decrease. The optimum atomic ratio of Ce/Ti was 0.5, and might be associated with the most efficient separation of photoinduced electron-hole pairs. Pleskov (1981) reported that the value of the space charge region potential for the efficient separation of electron-hole pairs should not be lower than 0.2 V. As the concentration of CeO_2 phase increased, the impurity band would become broader and, thus, the charge separation gap became narrower, and the recombination of electron-hole pairs was rapid. It could be seen that a stronger visible light absorbance with a higher cerium ion concentration did not lead to a higher photocatalytic activity, which might be limited by lower quantum efficiency (Li *et al.*, 2005b). The photocatalytic activities of all the samples were higher than those of P25 under UV irradiation.

As shown in Fig.10b, after 10 min of UV irradiation, the degradation of ARB were 69.5%, 72.2%, 86.5%, and 77.4% over $B_{0.0}Ce_{1.0}$-TiO_2, $B_{0.8}Ce_{1.0}$-TiO_2, $B_{1.6}Ce_{1.0}$-TiO_2, and P25, respectively. It indicated that the photocatalytic activities of the photocatalyst increased as the boron doping increased. The photocatalytic activity of the $B_{1.6}Ce_{1.0}$-TiO_2 sample was much higher than that of P25, whereas the photocatalytic activity of $B_{0.0}Ce_{1.0}$-TiO_2 and $B_{0.8}Ce_{1.0}$-TiO_2 was lower. It could be attributed to a reduction in the response of the sample to visible light and in the possible recombination of electron and hole pairs when boron was doped with TiO_2.

3 Conclusions

The experiment results showed that the prepared photocatalysts were mixed oxides consisting mainly of titania, ceria, and boron oxide. By comparison with pure TiO_2 prepared under the identical condition, the formation and growth of TiO_2 crystallites was inhibited when boron and cerium were doped. The XPS spectra of $B_{1.6}Ce_{1.0}$-TiO_2 calcined at 500°C showed that a few boron ions incorporated into TiO_2 lattice, whereas others existed as B_2O_3. Cerium ions existed as Ce^{3+} and Ce^{4+}, and the atomic ratio of Ce^{3+}/Ce^{4+} was 1.86. The UV-Vis absorbance band shifted toward the visible range (⩽526 nm) as TiO_2 was doped with the boron and cerium. The absorbance edge wavelength decreased as the calcination temperature was increased. The absorbance edge wavelength increased to 481 nm when the Ce/Ti atomic ratio was 1.0. For higher doping levels (Ce/Ti=2.0), the absorbance edge wavelength showed a slight decrease. The experiment results of ARB degradation indicated that the photocatalytic activities of boron- and cerium-codoped TiO_2 were affected drastically by solution pH, because of the change of surface charge. The activities of the samples increased with an enhancement of boron doping, whereas decreased when the Ce/Ti atom ratio was greater than 0.5. The optimum doping atomic ratio of B/Ti and Ce/Ti were 1.6 and 0.5, respectively.

References

Asahi R, Morikawa T, Ohwaki T *et al.*, 2001. Visible-light photocatalysis in nitrogen-doped titanium oxides[J]. Science, 293(5528): 269–271.

Bae E, Choi W, 2003. Highly enhanced photoreductive degradation of perchlorinated compounds on dye-sensitized metal/TiO_2 under visible light[J]. Environ Sci Technol, 37(1): 147–152.

Bensalem A, Bozon-Verduraz F, Delamar M *et al.*, 1995. Preparation and characterization of highly dispersed silica-supported ceria[J]. Appl Catal A, 121(1): 81.

Coronado J M, Maira A J, Martinez-Arias A *et al.*, 2002. EPR study of the radicals formed upon UV irradiation of ceria-based photocatalysts[J]. J Photochem Photobiol A, 150(1/2/3): 213–221.

Furube A, Asahi T, Masuhara H *et al.*, 1999. Charge carrier dynamics of standard TiO_2 catalysts revealed by femtosecond diffuse reflectance spectroscopy[J]. J Phys Chem B, 103(16): 3120–3127.

Galtayries A, Sporken R, Riga J *et al.*, 1998. XPS comparative study of ceria/zirconia mixed oxides: powders and thin film characterisation[J]. J Electron Spectrosc Relat Phenom, 88–91: 951–956.

Harris S J, Krauss G G, Simko S J *et al.*, 2002. Abrasion and chemical-mechanical polishing between steel and a sputtered boron carbide coating[J]. Wear, 252(1/2): 161–

169.

Hoffmann M R, Martin S T, Choi W Y *et al.*, 1995. Environmental applications of semiconductor photocatalysis[J]. Chem Rev, 95(1): 69–96.

Ishikawa A, Takata T, Kondo J N *et al.*, 2002. Oxysulfide $Sm_2Ti_2S_2O_5$ as a stable photocatalyst for water oxidation and reduction under visible light irradiation (lambda 650 nm)[J]. J Am Chem Soc, 124(45): 13547–13553.

Ishikawa A, Takata T, Matsumura T *et al.*, 2004. Oxysulfides $Ln_2Ti_2S_2O_5$ as stable photocatalysts for water oxidation and reduction under visible-light irradiation[J]. J Phys Chem B, 108(8): 2637–2642.

Jung K Y, Park S B, Ihm S K, 2004. Local structure and photocatalytic activity of B_2O_3-SiO_2/TiO_2 ternary mixed oxides prepared by sol-gel method[J]. Appl Catal B, 51(4): 239–245.

Kamat P V, 2002. Photophysical, photochemical and photocatalytic aspects of metal nanoparticles[J]. J Phys Chem B, 106(32): 7729–7744.

Khan S U M, Al-Shahry M, Ingler W B, 2002. Efficient photochemical water splitting by a chemically modified n-TiO_2[J]. Science, 297(5590): 2243–2245.

Li F B, Li X Z, 2002. Photocatalytic properties of gold/gold ion-modified titanium dioxide for wastewater treatment[J]. Appl Catal A, 228(1/2): 15–27.

Li F B, Li X Z, Ao C H *et al.*, 2005a. Enhanced photocatalytic degradation of VOCs using Ln^{3+}-TiO_2 catalysts for indoor air purification[J]. Chemosphere, 59(6): 787–800.

Li F B, Li X Z, Hou M F *et al.*, 2005b. Enhanced photocatalytic activity of Ce^{3+}-TiO_2 for 2-mercaptobenzothiazole degradation in aqueous suspension for odour control[J]. Appl Catal A, 285(1/2): 181–189.

Licht S, Wang B, Mukerji S *et al.*, 2000. Efficient solar water splitting, exemplified by Ru_2-catalyzed AlGaAs/Si photoelectrolysis[J]. J Phys Chem B, 104(38): 8920–8924.

Liu Z L, Guo B, Hong L *et al.*, 2005. Preparation and characterization of cerium oxide doped TiO_2 nanoparticles[J]. J Phys Chem Solids, 66(1): 161–167.

Lu G, Bernasek S L, Schwartz J, 2000. Oxidation of a polycrystalline titanium surface by oxygen and water[J]. Surf Sci, 458(1/2/3): 80–90.

Lu Y H, Zhou Z F, Sit P *et al.*, 2004. X-ray photoelectron spectroscopy characterization of reactively sputtered Ti-B-N thin films[J]. Surf Coat Technol, 187(1): 98–105.

Miyauchi M, Nakajima A, Watanabe T *et al.*, 2002. Photocatalysis and photoinduced hydrophilicity of various metal oxide thin films[J]. Chem Mater, 14(6): 2812–2816.

Ohno T, Akiyoshi M, Umebayashi T *et al.*, 2004. Preparation of S-doped TiO_2 photocatalysts and their photocatalytic activities under visible light[J]. Appl Catal A, 265(1): 115–121.

Otsuka-Yao-Matsuo S, Omata T, Yoshimura M, 2004. Photocatalytic behavior of cerium titanates, $CeTiO_4$ and $CeTi_2O_6$ and their composite powders with SrTiO3[J]. J Alloys Compd, 376(1/2): 262–267.

Park P W, Ledford J S, 1996. Effect of crystallinity on the photoreduction of cerium oxide: A study of CeO_2 and Ce/Al_2O_3 catalysts[J]. Langmuir, 12(7): 1794–1799.

Pleskov Y V, 1981. Conversion of luminous energy into electrical and chemical energy in photoelectrochemical cells with semiconductor electrodes (review)[J]. Soviet Electrochemistry, 17(1): 1–25.

Reddy B A, Khan A, Yamada Y *et al.*, 2002a. Surface characterization of CeO_2/SiO_2 and V_2O_5/CeO_2/SiO_2 catalysts by Raman, XPS, and other techniques[J]. J Phys Chem B, 106(42): 10964–10972.

Reddy B M, Sreekanth P M, Reddy E P *et al.*, 2002b. Surface characterization of La_2O_3-TiO_2 and V_2O_5/La_2O_3-TiO_2 catalysts[J]. J Phys Chem B, 106(22): 5695–5700.

Wang J A, Limas-Ballesteros R, Lopez T *et al.*, 2001. Quantitative determination of titanium lattice defects and solid-state reaction mechanism in iron-doped TiO_2 photocatalysts[J]. J Phys Chem B, 105(40): 9692–9698.

Ward M D, White J R. Bard A J, 1983. Electrochemical investigation of the energies of particulate titanium dioxide photocatalysts: The methyl viologen-acetate system[J]. J Am Chem Soc, 105(1): 27–31.

Xie Y B, Yuan C W, 2003. Photocatalytic activity and recycle application of titanium dioxide sol for X-3B photodegradation[J]. J Mol Catal A: Chem, 206(1/2): 419-428.

Xie Y B, Yuan C W, 2004. Visible light induced photocatalysis of cerium ion modified titania sol and nanocrystallites[J]. J Mater Sci Technol, 20(1): 14–18.

Xu A W, Gao Y, Liu H Q, 2002. The preparation, characterization, and their photocatalytic activities of rare-earth-doped TiO_2 nanoparticles[J]. J Catal, 207(2): 151–157.

Yakuphanoglu F, Arslan M, 2004. Determination of electrical conduction mechanism and optical band gap of a new charge transfer complex: TCNQ-PANT[J]. Solid State Commun, 132(3/4): 229–234.

Yu J G, Yu H G, Cheng B *et al.*, 2003. The effect of calcination temperature on the surface microstructure and photocatalytic activity of TiO_2 thin films prepared by liquid phase deposition [J]. J Phys Chem B, 107(50): 13871–13879.

Zhao W, Ma W H, Chen C C *et al.*, 2004. Efficient degradation of toxic organic pollutants with Ni_2O_3/$TiO_{2-x}B_x$ under visible irradiation[J]. J Am Chem Soc, 126(15): 4782–4783.